AIAA JOURNAL
Vol. 49, No. 7, July 2011

# Investigations of Lift-Based Pitch–Plunge Equivalence for Airfoils at Low Reynolds Numbers

Gregory Z. McGowan*
*North Carolina State University, Raleigh, North Carolina 27695-7910*
Kenneth Granlund† and Michael V. Ol‡
*U.S. Air Force Research Laboratory, Wright-Patterson Air Force Base, Ohio 45433-7542*
and
Ashok Gopalarathnam§ and Jack R. Edwards¶
*North Carolina State University, Raleigh, North Carolina 27695-7910*

DOI: 10.2514/1.J050924

**The limits of linear superposition in two-dimensional high-rate low-Reynolds-number aerodynamics are examined by comparing the lift-coefficient history and flowfield evolution for airfoils undergoing harmonic motions in pure pitch, pure plunge, and pitch–plunge combinations. Using quasi-steady airfoil theory and Theodorsen's formula as predictive tools, pitching motions are sought that produce lift histories identical to those of prescribed plunging motions. It follows that a suitable phasing of pitch and plunge in a combined motion should identically produce zero lift, canceling either the circulatory contribution (with quasi-steady theory) or the combination of circulatory and noncirculatory contributions (with Theodorsen's formula). Lift history is measured experimentally in a water tunnel using a force balance and is compared with two-dimensional Reynolds-averaged Navier–Stokes computations and Theodorsen's theory; computed vorticity contours are compared with dye injection in the water tunnel. Theodorsen's method evinces considerable, and perhaps surprising, resilience in finding pitch-to-plunge equivalence of lift-coefficient–time history, despite its present application to cases in which its mathematical assumptions are demonstrably violated. A combination of pitch and plunge motions can be found such that net lift coefficient is nearly identically zero for arbitrarily high reduced frequency, provided that amplitude is small. Conversely, cancellation is possible at large motion amplitude, provided that reduced frequency is moderate. The product of Strouhal number and nondimensional amplitude is therefore suggested as the upper bound for when superposition and linear predictions remain valid in massively unsteady two-dimensional problems.**

## Nomenclature

| | | |
|---|---|---|
| $a$ | = | $(x_p - c/2)/(c/2)$ |
| $b$ | = | one-half of the chord length |
| $C(k)$ | = | Theodorsen's function |
| $C_l$ | = | airfoil lift coefficient |
| $c$ | = | chord length |
| $F(k)$ | = | real part of the Theodorsen function |
| $G(k)$ | = | imaginary part of the Theodorsen function |
| $f$ | = | physical frequency |
| $h$ | = | plunge displacement |
| $K_0(ik)$ | = | Bessel function of the second kind, order zero |
| $K_1(ik)$ | = | Bessel function of the second kind, order one |
| $k$ | = | reduced frequency, $\omega c/(2V_\infty)$ |
| $M$ | = | freestream Mach number |
| $Re$ | = | freestream Reynolds number |
| $St$ | = | Strouhal number based on the peak-to-peak plunge amplitude, $2k(h_m/c)/\pi$ |
| $T$ | = | time period |
| $t$ | = | time |
| $V_\infty$ | = | freestream velocity |
| $x_p$ | = | chordwise distance from the leading edge to the pivot point |
| $\alpha$ | = | angle of attack |
| $\alpha_m$ | = | angle of attack in mean position |
| $\alpha_{0l}$ | = | zero-lift angle of attack |
| $\Gamma$ | = | bound circulation around the airfoil |
| $\Delta C_l$ | = | peak-to-peak amplitude of $C_l$ variation |
| $\theta$ | = | pitch-angle displacement |
| $\psi$ | = | phase shift for pitch |
| $\omega$ | = | circular frequency ($2\pi f$), spanwise vorticity |

*Subscripts*

| | | |
|---|---|---|
| $m$ | = | maximum displacement (amplitude) |
| $q$ | = | quasi-steady thin-airfoil-theory approach |
| ss | = | steady state |
| $t$ | = | Theodorsen's approach |
| $\infty$ | = | freestream conditions |

Presented as Paper 2009-0535 at the 47th AIAA Aerospace Sciences Meeting, Orlando, FL, 5–8 January 2009 and Paper 2010-8126 at the AIAA Atmospheric Flight Mechanics Conference, Toronto, Ontario, Canada, 2–5 August 2010; received 12 September 2010; revision received 11 February 2011; accepted for publication 22 February 2011. 

*Graduate Research Assistant, Department of Mechanical and Aerospace Engineering, Box 7910; currently Engineer, Corvid Technologies, Mooresville, NC. Member AIAA.

†Postdoctoral Scholar, Air Vehicles Directorate, Building 45, 2130 8th Street. Member AIAA.

‡Aerospace Engineer, Air Vehicles Directorate, Building 45, 2130 8th Street. Associate Fellow AIAA.

§Associate Professor, Department of Mechanical and Aerospace Engineering, Box 7910. Associate Fellow AIAA.

¶Professor, Department of Mechanical and Aerospace Engineering, Box 7910. Associate Fellow AIAA.

## I. Introduction

UNSTEADY aerodynamics, even in two dimensions and for rigid airfoils, continues to contain formidable challenges for problems of high reduced frequency, large amplitude, strong viscous and vortical effects, and large aerodynamic transients. Difficulties include the relationship between shed vortices and the

aerodynamic-force–time history, the limits of superposition and linearization, and the outlook for decomposition of arbitrary airfoil motions into elementary motions. The possible motions in two dimensions are vertical displacement or plunge, rotation or pitch (about a given pivot point, which is arbitrary but constant), and streamwise displacement. Ignoring for the present the streamwise displacement, one would like to assess in what sense pitch and plunge can be taken as equivalent, upon departure from small-amplitude linearizations where such equivalence is, of course, trivial. That is, for a high-frequency and moderate- or large-amplitude pure plunge, can a pure pitch be found, such that the lift-coefficient–time history would be the same? And if so, would a superposition where the pitch is subtracted from the plunge give an identically zero time-varying lift coefficient? And if lift-coefficient–time history is matched between the pitch and plunge, would the flowfield time history (that is, the various vortex-shedding events and the wake structure) also match?

Building on earlier studies by the authors [1–3], the current work uses an integrated analytical, computational, and experimental study of carefully selected pitch, plunge, and combination motions of an SD7003 airfoil [4] at a Reynolds numbers of 10,000. The SD7003 airfoil was selected instead of the venerable NACA 0012 because of the former's better suitability to low-Reynolds-number applications and because of interest in studying cases with net positive lift coefficient. The SD7003 has been the recent subject of detailed static measurements [5], low-frequency dynamic measurements/computations [6], and high-frequency measurements/computations [1]. Lift-based equivalence between pitch and plunge motions, defined as pitch and plunge motions that are predicted to result in the same $C_l(t)$, using closed-form solutions from analytical methods is used to bring out the relative importance of different contributions to the flow physics, while illustrating several interesting flow properties of the resulting pitch and plunge motions and their combinations. Closely related to pitch–plunge equivalence is pitch–plunge cancellation, which results when the combination of a pitch motion with a plunge motion is predicted to result in zero $C_l(t)$. Two analytical approaches are used to determine equivalent pitch and plunge motions: quasi-steady thin-airfoil theory (QSTAT) and Theodorsen's theory. These approaches were chosen because they model the unsteady aerodynamics with increasing fidelity by including additional flow-physics contributions: going from QSTAT to Theodorsen's theory, the effects of noncirculatory contributions and wake vorticity are included. In the current work, pitch and plunge motion pairs, determined to be equivalent using these two approaches, are studied using analytical (Theodorsen's method [7]), computational [using CFL3D [8], a Reynolds-averaged Navier–Stokes (RANS) code], and experimental (force measurements and dye-flow visualization in a water tunnel [9]) methods. In so doing, we mutually compare theory, computation, and experiment. We vary plunge amplitude, pitch amplitude, and pivot-point location for a range of reduced frequencies in an attempt to cover the parameters necessary for assessment of the bounds of linear theory in predicting the lift history for highly unsteady, separated flows.

## II. Motion Parameters

Figure 1 provides an illustration of pure-plunge and pure-pitch motions for an airfoil with a mean angle of attack of $\alpha_m$. The plunge and pitch displacements, denoted by $h$ and $\theta$, respectively, have amplitudes of $h_m$ and $\theta_m$, respectively, in sinusoidal motion. The chordwise distance of the pivot point (for pitch) from the leading edge is denoted by $x_p$. If the frequency of oscillation is $f$ (time period is $T$) and the circular frequency $\omega$ is $2\pi f$, the reduced frequency $k$ is defined as $k = \omega c/(2V_\infty)$. Additionally, following typical usage in unsteady airfoil aerodynamics, $b = c/2$ and $a = (x_p - c/2)/(c/2)$.

For sinusoidal pure-plunge motion, Eq. (1) presents the expressions for time variations of plunge displacement $h$, plunge velocity $\dot{h}$, and plunge acceleration $\ddot{h}$, as follows:

$$h = h_m e^{i\omega t} \qquad \dot{h} = i\omega h_m e^{i\omega t} \qquad \ddot{h} = -\omega^2 h_m e^{i\omega t} \tag{1}$$

Likewise, for sinusoidal pure-pitch motion, Eq. (2) presents the expressions for time variations of pitch angle $\theta$, pitch rate $\dot{\theta}$, and pitch acceleration $\ddot{\theta}$. The pitch motion is assumed to have a phase lead angle of $\psi$:

$$\begin{aligned}\theta &= \theta_m e^{i(\omega t+\psi)} = \theta_m e^{i\omega t} e^{i\psi}\\ \dot{\theta} &= i\omega\theta_m e^{i(\omega t+\psi)} = i\omega\theta_m e^{i\omega t} e^{i\psi}\\ \ddot{\theta} &= -\omega^2\theta_m e^{i(\omega t+\psi)} = -\omega^2\theta_m e^{i\omega t} e^{i\psi}\end{aligned} \tag{2}$$

## III. Analytical Approaches to Pitch–Plunge Matching

In this section, two approaches for pitch–plunge matching are presented. The approaches are 1) lift matching using QSTAT and 2) lift matching using Theodorsen's theory. A good review of the QSTAT and Theodorsen's theory is given by Leishman [10].

Before discussing the details of the two approaches, it is useful to first consider the expressions for $C_l(t)$ from the two theories for combined pitch–plunge motions. Using the subscripts $q$ and $t$, respectively, to denote the results from the QSTAT and Theodorsen's theory, the expressions for $C_l$ in terms of the steady-state plunge and pitch contributions are

$$C_{lq} = C_{l\text{ss}} + C_{l\text{plunge},q} + C_{l\text{pitch},q} \tag{3}$$

and

$$C_{lt} = C_{l\text{ss}} + C_{l\text{plunge},t} + C_{l\text{pitch},t} \tag{4}$$

where the steady-state contribution (for either theory), $C_{l\text{ss}}$, resulting from the mean and zero-lift angles of attack, $\alpha_m$ and $\alpha_{0l}$, can be written as

$$C_{l\text{ss}} = 2\pi(\alpha_m - \alpha_{0l}) \tag{5}$$

Ignoring the steady-state contribution, which can be added later, the $C_l$ from QSTAT due to plunge and pitch contributions can be written as

$$C_{lq} = 2\pi\left[-\frac{\dot{h}}{V_\infty} + \theta + b\left(\frac{1}{2} - a\right)\frac{\dot{\theta}}{V_\infty}\right] \tag{6}$$

and the $C_l$ from Theodorsen's theory due to plunge and pitch contributions is

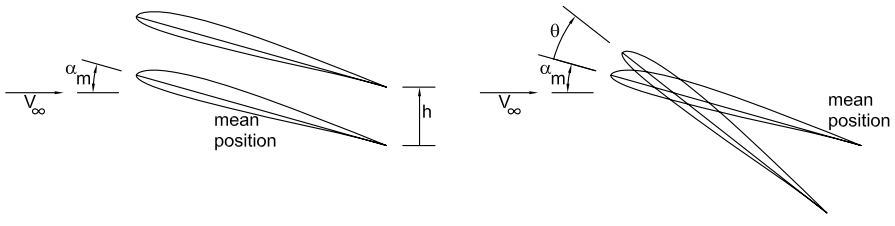


**Fig. 1 Pitch and plunge definitions. Plunge and pitch displacements are positive as shown.**

$$C_{lt} = \pi b\left(-\frac{\ddot{h}}{V_\infty^2} + \frac{\dot{\theta}}{V_\infty} - ba\frac{\ddot{\theta}}{V_\infty^2}\right) + 2\pi C(k)\left[-\frac{\dot{h}}{V_\infty} + \theta + b\left(\frac{1}{2} - a\right)\frac{\dot{\theta}}{V_\infty}\right] \tag{7}$$

We note that the resultant aerodynamic force in inviscid flow in a plunging motion is generally not in the same direction as that for a pitching motion. However, as long as we are interested in the lift force, i.e., in the component of the resultant force that is in the direction perpendicular to $V_\infty$, and the lift coefficient is defined using $V_\infty$ as the reference velocity, the expressions for $C_l$ due to pitch and plunge may be added without any loss of generality. Although the expressions for $C_l$ due to pitch and plunge in Eqs. (6) and (7) are derived using small-angle approximations, their directions are always perpendicular to $V_\infty$, even when the small-angle assumptions are violated.

In Eq. (7), the first term on the right side of the equation is the lift from the noncirculatory effects. The second term on the right side is the lift from circulatory effects and is similar to the corresponding lift contributions shown from QSTAT, except for the factor of $C(k)$, which is known as Theodorsen's function. For a given $k$, $C(k)$ is a complex number that brings into consideration the effect of the wake vorticity on the flow induced at the airfoil. Thus, Theodorsen's method includes two flow-physics contributions not modeled by QSTAT: the fluid-acceleration effects through the noncirculatory terms and the effects of the vorticity distribution in the planar wake through $C(k)$. The exact expression for Theodorsen's function is given in Eq. (8), in which $K_0(ik)$ and $K_1(ik)$ are the modified Bessel functions of the second kind, of orders zero and one, respectively:

$$C(k) = F(k) + iG(k) = \frac{K_1(ik)}{K_0(ik) + K_1(ik)} \tag{8}$$

In the search for approaches to determine equivalent pitch and plunge motions, the effort turned to the use of QSTAT and Theodorsen's theory to determine pitch and plunge motions that would give the same $C_l(t)$. Associated with pitch–plunge equivalence is the idea of pitch–plunge cancellation, where pitch and plunge motions are selected to result in a net zero $C_l(t)$. Examining Eqs. (6) and (7), it is clear that if QSTAT is used for pitch–plunge cancellation, the resulting motion, when examined using Theodorsen's theory, would have zero circulatory contribution to lift and any resulting lift would be due to noncirculatory contributions. On the other hand, if Theodorsen's theory is used for pitch–plunge cancellation, the resulting motion should have zero net lift from both circulatory and noncirculatory contributions. Assuming that these two motions could be constructed, the questions were as follows:

1) Would these motions indeed result in lift cancellation for moderate to high reduced frequencies and amplitudes at low Reynolds numbers?

2) What would the effect be on the resulting flowfields (vortex shedding, wake structure, etc.)?

The following subsections present the derivations of the pitch–plunge matching/cancellation approaches using QSTAT and Theodorsen's theory.

### A. QSTAT Approach

In this subsection, QSTAT is used to match the $C_l(t)$ for pitch with the $C_l(t)$ for plunge. Pitch–plunge equivalence with this approach, $C_{l\text{plunge},q}(t) = C_{l\text{pitch},q}(t)$, results in

$$-\frac{\dot{h}}{V_\infty} = \theta + b\left(\frac{1}{2} - a\right)\frac{\dot{\theta}}{V_\infty} \tag{9}$$

which simplifies to

$$-2ik\frac{h_m}{c} = \theta_m\left[1 + ik\left(\frac{1}{2} - a\right)\right](\cos\psi + i\sin\psi) \tag{10}$$

Equating the real parts of the left and right sides of Eq. (10) yields the following expression for $\psi$:

$$\psi = \tan^{-1}\left[\frac{1}{\left(\frac{1}{2} - a\right)k}\right] \tag{11}$$

Equating the imaginary parts of Eq. (10) yields the following expression for the ratio of pitch amplitude to plunge amplitude:

$$\frac{\theta_m}{h_m/c} = \frac{-2k}{\left(\frac{1}{2} - a\right)k\cos\psi + \sin\psi} \tag{12}$$

It is shown that the $\psi$ required for equivalence is independent of the amplitude of the motion and is dependent only on $k$ and the pivot location. Once $\psi$ is determined from Eq. (11), the ratio of pitch amplitude to plunge amplitude can be determined from Eq. (12). It is also shown that when the pivot location is at three-quarter-chord (i.e., when $a = 1/2$), the effect of pitch rate vanishes.

Instead of pitch–plunge lift equivalence, pitch–plunge lift cancellation can be achieved by combining pitch and plunge motions such that $C_{l\text{plunge},q}(t) + C_{l\text{pitch},q}(t) = 0$. For any given plunge motion, it turns out that the motion parameters ($\psi$ and $\theta_m$) for pitch that will result in lift cancellation from QSTAT are identical to those for lift equivalence, with the exception of a sign reversal on the quantity $\theta_m$.

### B. Theodorsen Approach

In this approach, Theodorsen's method [7] is used to match the $C_l(t)$ for pitch with the $C_l(t)$ for plunge. For pitch–plunge equivalence with this approach, $C_{l\text{plunge},t}(t)$ is set equal to $C_{l\text{pitch},t}(t)$. Substituting the expressions for $h$ and $\theta$ and their time derivatives from Eqs. (1) and (2) results in a lengthy complex expression. Equating the real parts of the left and right sides of this expression yields

$$2k(k + 2G)\frac{h_m}{c} = \left[-k\sin\psi + k^2a\cos\psi + 2F\cos\psi - 2G\sin\psi - 2k\left(\frac{1}{2} - a\right)(F\sin\psi + G\cos\psi)\right]\theta_m \tag{13}$$

and equating the imaginary parts yields

$$-4kF\frac{h_m}{c} = \left[k\cos\psi + k^2a\sin\psi + 2G\cos\psi + 2F\sin\psi + 2k\left(\frac{1}{2} - a\right)(F\cos\psi - G\sin\psi)\right]\theta_m \tag{14}$$

By dividing Eq. (13) by Eq. (14) and dividing the numerator and denominator of the right side of the resulting expression by $\cos\psi$, the following closed-form expression for the phase angle $\psi$ results:

$$\psi = \tan^{-1}\left(\frac{C - AB}{AC + B}\right) \tag{15}$$

where $A$, $B$, and $C$ are

$$A = \frac{k + 2G}{-2F} \tag{16}$$

$$B = k + 2G + 2k\left(\tfrac{1}{2} - a\right)F \tag{17}$$

and

$$C = k^2a + 2F - 2k\left(\tfrac{1}{2} - a\right)G \tag{18}$$

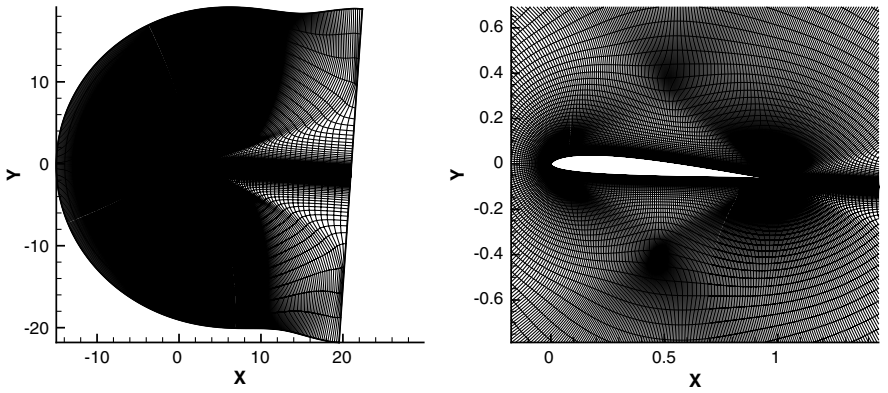


**a) Entire grid** **b) Close up**

**Fig. 2 Depiction of grid used for CFL3D simulations with moving-grid capability.**

Similar to the QSTAT approach, it is shown that $\psi$ is independent of the motion amplitude and is dependent only on $k$ and the pivot location. For a given $k$ and $a$, the $\psi$ determined from Eq. (15) can be substituted in either Eq. (13) or Eq. (14) to determine the ratio of pitch amplitude to plunge amplitude, $\theta_m/(h_m/c)$, required for pitch–plunge equivalence using Theodorsen's approach. As discussed for the QSTAT approach, when pitch–plunge cancellation is desired, $C_{l\text{pitch},t} + C_{l\text{plunge},t}$ is set equal to zero. For this case, $\psi$ is the same as that determined using Eq. (15), but the $\theta_m/(h_m/c)$ is the exact negative of that determined for pitch–plunge equivalence.

## IV. Computational Modeling Using CFL3D

CFL3D [8] is a research code developed at the NASA Langley Research Center that solves the thin-layer Navier–Stokes equations. The CFL3D code is a robust flow solver that has been used by many researchers for a wide range of applications. It is written in the structured framework and is capable of calculating solutions on one-to-one, patched, or overset grids. CFL3D also includes convergence-acceleration techniques: namely, local time-step scaling, grid sequencing, and multigrid. It also includes built-in routines to accommodate grid motions, including grid deformations; with these, simple motions (such as translations and rotations) and complicated motions (such as deforming surfaces and other aeroelastic type motions) can be solved. Although several turbulence models are built into the CFL3D code, the current research uses only the Spalart–Allmaras [11] turbulence model. This turbulence model was used simply because the choice of turbulence model for this problem is largely irrelevant; for example, in Ol et al. [12], the $k$-$\omega$ turbulence model was used. Additionally, in a study of a plunging airfoil using high-fidelity implicit large-eddy simulations, Visbal [13] observed that transitional effects were minimal for $Re = 10,000$. Earlier work by McGowan et al. [1] showed that Reynolds number effects were also negligible between $Re = 10,000$ and 40,000 for pitch and plunge motions similar to those studied in the current work.

In this work, all computations were for two-dimensional flow, using the grid shown in Fig. 2. This 2-D grid consists of 689 nodes in the $i$ direction (around the airfoil surface) and 113 nodes in the $k$ direction (normal to the airfoil). A denser spacing near the airfoil surface was used to accurately predict boundary-layer effects. The outer domains of this grid extend to approximately 20 chords radially away from the airfoil in all directions. Unsteady motions using this grid were performed using the grid-motion technique implemented in CFL3D [14]. In this technique, the entire grid moves to simulate the desired motion. This grid was selected based on a sensitivity study discussed in [15]. Also presented in [15] are comparisons of results from CFL3D for various pitch and plunge motions with results from other computations and experiments in the literature.

The computations were run at a Mach number of 0.05 instead of the higher incompressible value of 0.2 used initially [2]. For high-reduced-frequency motions, the Mach number must be low enough to not violate the condition $Mk \ll 1$ [10,16] and introduce compressibility effects. If the condition is violated it can produce lift from a plunge oscillation motion at the correct amplitude at a phase lag of up to 90 deg [3], shown in Fig. 3. However, lift can still be canceled fairly well from a pitch–plunge combination motion [2] due to phase lag from both the pitching and plunging. To achieve computational stability at this low Mach number, low-speed preconditioning [17] was used.

## V. Experimental Setup

### A. Facility and Motion Mechanism

The U.S. Air Force Research Laboratory's horizontal free-surface water tunnel is fitted with a three-degree-of-freedom electric motion rig enabling independent control of pitch or rotation, plunge or heave, and surge or streamwise-aligned translation. Photographs of the tunnel and the model installation are shown in Fig. 4. More detail on the rig operation is given in Ol et al. [12], and the facility is discussed in Ol et al. [5].

The motion rig is operated through a Galil Motion Control DMC-4040 Ethernet-based controller, running a triplet of H2W electric linear rail positioning stages. Airfoil pitch and plunge are controlled via a pair of motors mounted vertically on a plate above the tunnel test section, shown in the left portion of Fig. 4. Each motor actuates a vertical plunge rod, which connects via a bushing to a coupler piece

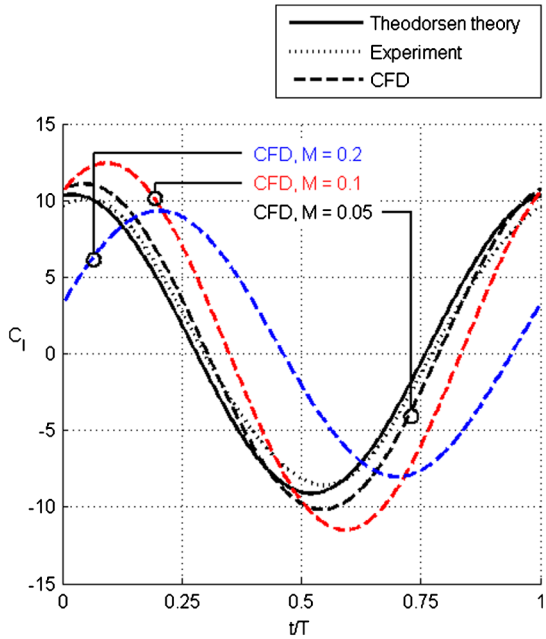


**Fig. 3 $C_l(t)$ distributions from CFD for freestream Mach numbers of 0.2, 0.1, and 0.05 compared with theory and experiment for a pure-plunge motion with $k = 7.86$, $Re = 10,000$, and $h_m/c = 0.025$.**

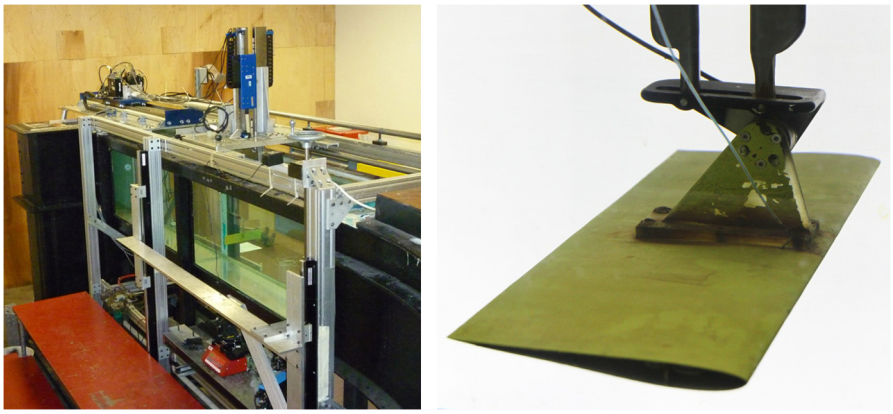

**Fig. 4 Test section and portion of motion rig mounted above test section of the U.S. Air Force Research Laboratory's horizontal free-surface water tunnel (left). SD7003 airfoil with force balance mounted between steel coupler piece and plastic foot connecting to the airfoil (right). Dye injection is from a 0.5-mm-diam slot at the airfoil leading edge, three-fourths spanwise location.**

holding the force balance. The upstream plunge rod is constrained to move purely vertically, whereas the downstream plunge rod is allowed to pivot in the test-section vertical plane of symmetry. The pitch pivot point can be varied by suitable choice of phase and amplitude difference in trajectory of front or rear plunge rod. For all cases in which the pitch pivot point is not coincident with the bushed end of the front plunge rod, there will be a parasitic streamwise displacement of the airfoil, which will be unavoidable unless the front plunge rod is allowed to pivot similarly to the downstream one. This is removed using the third degree of freedom, surge, which also actuates the fore and aft translating motions of the model. Surge is achieved using a larger linear motor mounted horizontally aft of the pitch–plunge carriage, with 48 in. peak-to-peak stroke and nominal speed up to 1 m/s.

The desired theoretical pitch and/or plunge histories of the airfoil are converted to position commands for each linear motor. Commanded-vs-attained displacement histories of the three motors are compared by interrogating the three motors' optical encoder tapes at 5000 increments/mm for the two vertical motors and at 1000 increments/mm for the streamwise motor. Peak discrepancies between commanded and attained positions are $300 \pm 100$ increments, which converts to 0.15 deg peak error in incidence angle if the two vertical motors' displacement errors are in the worst-case scenario of antiphase. However, this is the incidence-angle error at the force-balance location and does not account for vibration or elastic deflection of the plastic coupler piece between the force balance and the airfoil model. Manual interrogation of particle image velocimetry raw images in Ol et al. [12] (not reported here) showing reflection of laser light from the airfoil suction side implies an upper bound of incidence-angle uncertainty of 0.2 deg.

### B. Flow Visualization

Flow visualization was achieved by injection of mixture of blue food-coloring ink and ethanol, to match the density of the water, through a 0.5-mm-i.d. wand, exiting near the stagnation point at the three-fourths spanwise location. Wherever possible, the dye exit speed was matched to the freestream (6.6 cm/s), but in the larger-amplitude motions the dye exit speed was as high as 15 cm/s, to improve image contrast. Images were taken with a pco.dimax camera with a 2k × 2k complementary metal-oxide semiconductor array at 50 frames/s. The camera was fitted with a Nikon 35 mm camera lens with 20 mm focal length and arranged such that the suction side of the airfoil would be visible for the full range of airfoil pitch and plunge motions, which obscured the pressure side in some cases.

The overall objective in the flow visualization is to compare concentrations of shed vorticity with those of the computations, for validation of the latter. Of course, the visualizations capture only the evolution of a passive scalar dye concentration, not the vorticity vector field. Presently, the distinction can be regarded as small, however, at least for the initial evolution of the shed vortices (leading-edge vortices and near wake behind the trailing edge), from the argument that the advection term initially dominates the stretching term in the scalar (or vorticity) transport equation [18].

### C. Force Measurements

Force measurements used a Nano25 (ATI Industrial Automation, Inc.) waterproof six-component balance (right-hand image in Fig. 4), oriented to align its maximally sensitive channels with the longitudinal forces and moments (lift, drag, and pitching moment). For maximal force-balance sensitivity and reduction of vibrations, the balance should be at the model's center of pressure. This introduces unacceptable interference, however. A suitable alternative and a hydrodynamically cleaner arrangement is an aft sting, where the model is mounted some distance ahead of the balance, and the balance is integrated into a housing that connects to the two vertical plunge rods. Here, one must be careful about the stiffness of the sting and the balance itself. The apparent mass of the water accelerated along with the model (equal to a circular cylindrical slug of water, with the length being the same as the span of the model and the diameter equal to the model's chord) can be 10 times larger than that of the model, sting, and metric portion of the balance. Because the limiting measurement component of the balance is the pitching moment, an aft-sting arrangement was eschewed in favor of the configuration shown in Fig. 4, with the balance atop a plastic coupler piece connecting to the pressure side of the airfoil.

The balance signal was sampled at 100 Hz for 20 cycles of motion, phase-averaged, and low-pass-filtered at 10 Hz, with the first 10 cycles discarded from the phase average to avoid startup transients; 10 Hz was chosen as the filter cutoff, because the balance-coupler-model structural resonance frequency was approximately 14 Hz. This can be compared with a physical oscillation frequency of $\approx$0.5 Hz for sinusoidal pitch–plunge at $k = 4$. The tare procedure does not include a wind-off dynamic measurement, because this would corrupt measurement of noncirculatory aerodynamic force if forces were recorded with the tunnel filled with water, but with the tunnel's pump turned off, whereas the structural response of the balance would be different if the water was drained and air measurements were subtracted from water data. Instead, a pump-off (but tunnel-filled) static alpha sweep is taken. This is the static tare, and values from the static sweep are subtracted from the wind-on run, according to the respective geometric incidence angle of the airfoil in the wind-on run. This leaves the dynamic tare contribution. The airfoil model (with chord of 152.4 mm and wall-to-wall span of 457 mm) is made of stainless steel (0.75-mm-thick skin) with internal bracing. Because the model is partially hollow, it fills with water when submerged. The model was weighed together with its enclosed volume of water, and this mass, taken at the airfoil center of mass, produces a force and moment history at the balance center, in the $F = ma$ sense. This is calculated analytically for all prescribed airfoil pitch–plunge trajectories, and the vertical component is subtracted from the measured wind-on lift.

## VI. Results

We consider seven case studies listed in Table 1, Four cases are at a low Strouhal number of 0.125 and three at a high Strouhal number of 0.375, forming two Strouhal number families, as shown in Fig. 5. This selection of Strouhal number is motivated by observations in zoology that flapping flight in nature is often in the Strouhal number range of 0.2–0.4 [19]. In each Strouhal number family, we consider high-frequency/small-amplitude and low-frequency/large-amplitude motions. In all cases, the SD7003 airfoil is considered at a mean angle of attack $\alpha_m$ of 4 deg and a freestream Reynolds number of 10,000. Each case has a baseline motion: pure plunge. This is compared with pure pitch from quasi-steady airfoil theory, pure pitch from Theodorsen's formula, and pitch–plunge cancellation combinations from quasi-steady theory and from Theodorsen's formula.

Case 1 has $k = 3.93$ and $h_m/c = 0.05$. This was motivated by the seminal study of Platzer et al. [20] on high-frequency pure plunge of the NACA 0012 airfoil, with applications to flapping-wing flight of micro air vehicles. Case 1 seeks an equivalent pitch with pivot about the quarter-chord. Since quasi-steady airfoil theory predicts that pivot about the three-quarter-chord annihilates the pitch-rate contribution to lift history, case 2 seeks an equivalent pitch about the three-quarter-chord point, with the same baseline plunge motion as in case 1. In case 3, $k$ is reduced to 0.393 and $h_m/c$ is increased to 0.50. This is a comparatively slow large-amplitude case, in contradistinction to cases 1–2, in which noncirculatory forces are small and separation from the airfoil's suction side is expected to be large. Going the other way, in case 4 $k$ is increased to 7.86, which is twice that of case 1, and $h_m/c$ is reduced to 0.025, which is half of that used in case 1.

Case 5 begins the high-Strouhal-number family, with $k = 1.179$ and $h_m/c = 0.50$, taking the large-amplitude motion of case 3 to three times the frequency. Cases 6 and 7 return to the reduced frequencies of cases 1 and 4, respectively, but again with three times the respective plunge amplitude.

### A. Case Study 1

In this case study, $k = 3.93$ and the baseline pure-plunge motion has $h_m/c$ of 0.05. This pure-plunge motion was studied in detail computationally and experimentally in earlier work by the authors [1]. For this plunge motion, the equivalent pure-pitch motion for rotation about the quarter-chord location was determined using the two approaches: QSTAT and Theodorsen. Detailed motion parameters for all seven case studies are tabulated in Table 1.

The baseline plunge and the two pitch motions were analyzed using CFL3D and studied experimentally. The variations of $C_l(t/T)$ from Theodorsen's theory, CFL3D, and experiments for the baseline pure-plunge motion are shown in Fig. 6a and those for the two pure-pitch motions are shown in Fig. 6b.

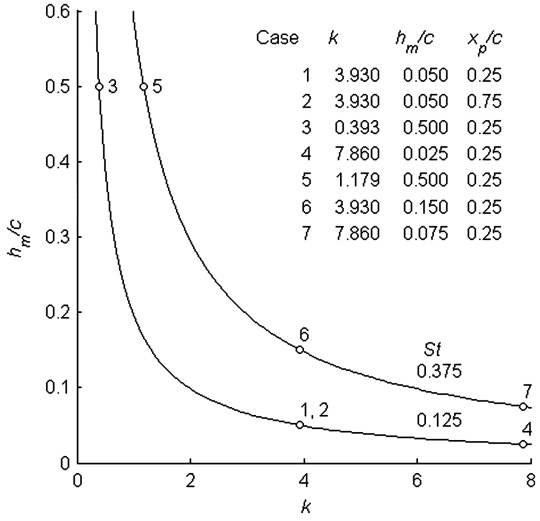


**Fig. 5 Values of reduced frequency and nondimensional plunge amplitude for seven cases, shown along with two curves of Strouhal number in the $k$–$h_m/c$ plane.**

**Table 1 Motion parameters for the seven case studies**

| Case[a] | Motion | Approach | $h_m/c$ | $\theta_m$, deg | $\psi$, deg |
|---|---|---|---|---|---|
| | *Case 1:* $k = 3.93$, $C(k) = 0.50–0.031i$, $x_p/c = 0.25$ | | | | |
| 1A | Pure plunge | —— | 0.05 | —— | —— |
| 1D | Pitch–plunge | QSTAT | 0.05 | 5.6 | 14.3 |
| 1E | Pitch–plunge | Theodorsen | 0.05 | 8.9 | 35.8 |
| | *Case 2:* $k = 3.93$, $C(k) = 0.50–0.031i$, $x_p/c = 0.75$ | | | | |
| 1A/2A | Pure plunge | —— | 0.05 | —— | —— |
| 2-D | Pitch–plunge | QSTAT | 0.05 | 22.5 | 90.0 |
| 2E | Pitch–plunge | Theodorsen | 0.05 | 9.4 | 141.5 |
| | *Case 3:* $k = 0.393$, $C(k) = 0.63–0.166i$, $x_p/c = 0.25$ | | | | |
| 3A | Pure plunge | —— | 0.5 | —— | —— |
| 3-D | Pitch–plunge | QSTAT | 0.5 | 21.0 | 68.6 |
| 3E | Pitch–plunge | Theodorsen | 0.5 | 19.9 | 69.8 |
| | *Case 4:* $k = 7.86$, $C(k) = 0.50–0.016i$, $x_p/c = 0.25$ | | | | |
| 4A | Pure plunge | —— | 0.025 | —— | —— |
| 4D | Pitch–plunge | QSTAT | 0.025 | 2.9 | 7.3 |
| 4E | Pitch–plunge | Theodorsen | 0.025 | 5.3 | 20.6 |
| | *Case 5:* $k = 1.179$, $C(k) = 0.53–0.089i$, $x_p/c = 0.25$ | | | | |
| 5A | Pure plunge | —— | 0.5 | —— | —— |
| 5D | Pitch–plunge | QSTAT | 0.5 | 43.7 | 40.3 |
| 5E | Pitch–plunge | Theodorsen | 0.5 | 42.4 | 57.7 |
| | *Case 6:* $k = 3.93$, $C(k) = 0.50–0.031i$, $x_p/c = 0.25$ | | | | |
| 6A | Pure plunge | —— | 0.15 | —— | —— |
| 6D | Pitch–plunge | QSTAT | 0.15 | 16.7 | 14.3 |
| 6E | Pitch–plunge | Theodorsen | 0.15 | 26.6 | 35.8 |
| | *Case 7:* $k = 7.86$, $C(k) = 0.50–0.016i$, $x_p/c = 0.25$ | | | | |
| 7A | Pure plunge | —— | 0.075 | —— | —— |
| 7D | Pitch–plunge | QSTAT | 0.075 | 8.53 | 7.3 |
| 7E | Pitch–plunge | Theodorsen | 0.075 | 15.9 | 20.6 |

[a]Pure plunge (A) and pitch–plunge combinations for lift cancellation using the QSTAT (D) and Theodorsen (E) approaches. Pure-pitch motions for lift equivalence using QSTAT (B) and Theodorsen (C) approaches can be determined from D and E, respectively, by setting $h_m/c = 0$ and reversing the sign of $\theta_m$.

Examining the results for the pure-plunge motion first, excellent agreement is shown between theory, computational fluid dynamics (CFD), and experiments. The peak-to-peak amplitude of $C_l$ ($\Delta C_l$) is approximately 9.8, with a mean value of approximately 0.7. The mean value corresponds to $C_{lss}$, which is consistent with $\alpha_m$ of 4 deg and $\alpha_{0l}$ of approximately $-2$ deg. Examining the $C_l(t/T)$ for the two pitch cases next, excellent agreement is shown for the QSTAT-derived motion, case 1B. For the Theodorsen-derived pitch motion, case 1C, CFD, and experiment, although in good agreement with each other, deviate from theoretical predictions by approximately 20% for approximately a quarter-cycle around the positive and negative peaks.

It is shown that the $C_l(t/T)$ distributions for the QSTAT-derived pitch case have a peak-to-peak amplitude, $\Delta C_l$ of 5.8, which does not match the $\Delta C_l$ values for the pure-plunge distributions. This observation is easily explained by recognizing that the QSTAT-derived pitch motion matches only the circulatory component of the lift force from the plunge motion. The total $C_l$, composed of circulatory and noncirculatory components, cannot be expected to match between the plunge and the QSTAT-derived pitch motions. For the Theodorsen-derived pitch motions, the $\Delta C_l$ is 9.8 from theory, approximately 11.0 from CFD, and 10.0 from experiment. Comparison of the results in Figs. 6a and 6b shows that the $C_l$ distributions for the plunge and the Theodorsen-derived pitch motions compare well in both amplitude and phase. When Theodorsen's formula is used for pitch–plunge matching, both circulatory and noncirculatory effects are captured, which explains the good match between the $C_l$ distributions.

To gain further understanding of the issues involved in the pitch–plunge equivalence, plots of the vorticity field from CFD and snapshots from dye-flow visualization from experiment are examined for the three motions for $t/T$ of 0 and 0.5 in Fig. 7. First, we note that the vorticity-field plots from CFD for all three motions are in excellent qualitative agreement with the corresponding

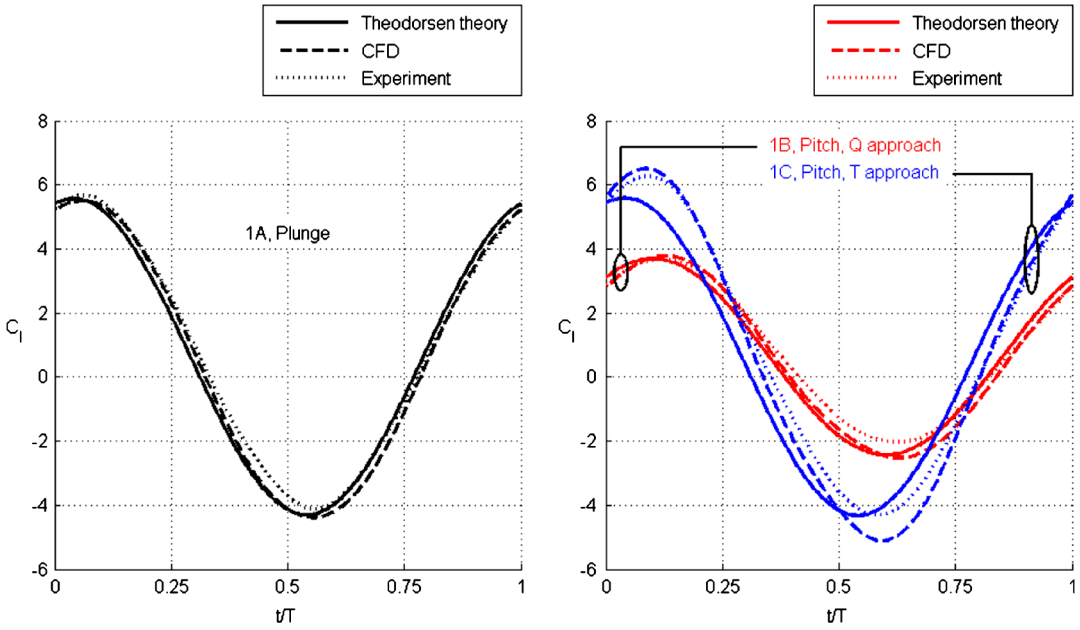


**a) Pure plunge** **b) Pure pitch**

**Fig. 6** $C_l(t)$ **distributions from Theodorsen's theory, CFD, and experiment in case 1. Q approach and T approach in this and the following figures refer to the QSTAT and Theodorsen approaches, respectively.**

dye-flow snapshots from experiment, especially for the locations of the vortices in the wake. Comparing the CFD vorticity-field plots and the dye-flow snapshots for the QSTAT-derived pitch case (second row) with those for the baseline plunge case (first row) shows that the flowfields for the two motions are remarkably similar, especially in the wake region. Comparing the CFD vorticity-field plots and the dye-flow snapshots for the Theodorsen-derived pitch case (third row) with the corresponding plunge plots, it is shown that there is reasonable comparison between the wake flow and excellent comparison of the surface flow features.

It is interesting to note that the agreement with the plunge $C_l(t/T)$ is much better for the Theodorsen-derived pitch motion than for the QSTAT-derived pitch motion. On the other hand, the agreement with the wake vorticity of the plunge is slightly better for the QSTAT pitch motion than for the Theodorsen pitch motion.

To better evaluate the effectiveness of the QSTAT and Theodorsen approaches, combined pitch–plunge motions were generated for pitch–plunge cancellation; these motions were then studied using Theodorsen's theory, CFD, and experiment. As mentioned earlier, pitch–plunge cancellation aims to set $C_{l\text{plunge}} + C_{l\text{pitch}} = 0$. The pitch motion used for cancellation has the same parameters as those used for pitch–plunge equivalence, with the exception of a sign reversal on $\theta_m$ .

Figure 8 shows the $C_l(t/T)$ variations from theory, CFD, and experiment for the QSTAT- and Theodorsen-derived combined pitch–plunge motions and for the baseline pure-plunge motion. For all three motions, there is good agreement between theory, CFD, and experiment. It is shown that the QSTAT-derived pitch–plunge motion has a $\Delta C_l$ of around 5.0, showing that this approach is not successful at achieving lift cancellation. This is because the QSTAT approach results in a cancellation of only the circulatory portion of the lift; the noncirculatory portion of the lift does not get canceled. The net $C_l$ distribution for the QSTAT-derived pitch–plunge motion is therefore the noncirculatory $C_l$ variation superposed on the constant steady-state value of $C_{l_{ss}}$. On the other hand, the Theodorsen-derived pitch–plunge motion has a $\Delta C_l$ of only 0.6 from CFD and 1.1 from experiment, which is a small percentage (6% from CFD and 10% from experiment) of the $\Delta C_l$ values from CFD and experiment,

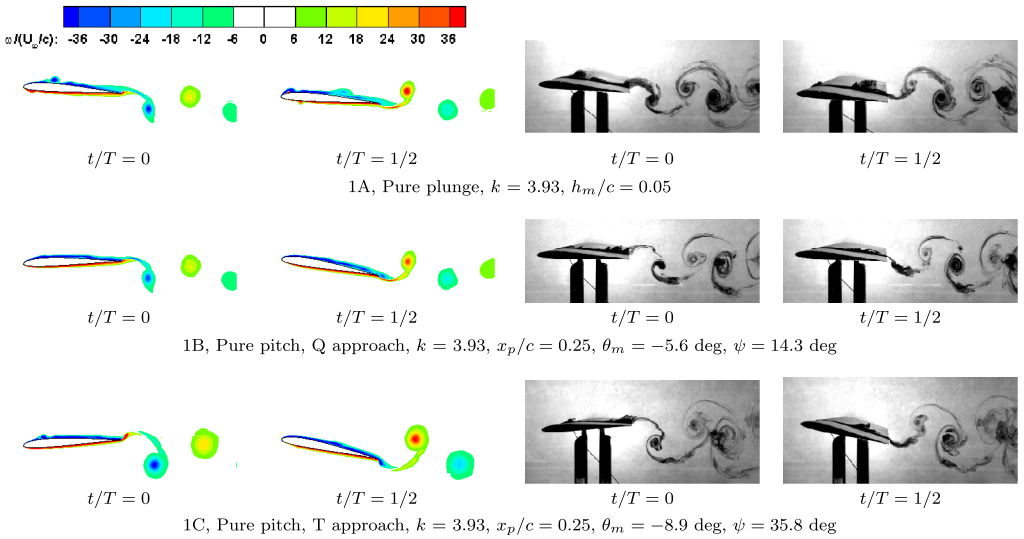


**Fig. 7 Cases 1A, 1B, 1C: Vorticity-field plots from CFD (left), dye-flow visualization (right).**

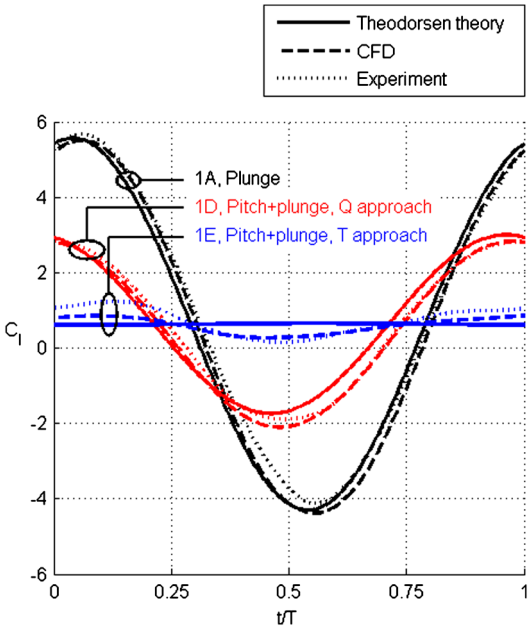


**Fig. 8 $C_l(t)$ distributions from Theodorsen's theory, CFD, and experiment for the baseline pure-plunge motion and the two pitch–plunge combination motions in case 1.**

respectively, for the pure-plunge case. From this we can conclude that the Theodorsen approach to pitch–plunge cancellation is remarkably successful.

Figure 9 presents the vorticity-field plots from CFD and the dye-flow visualization snapshots from experiment for the two combined pitch–plunge motions. For both motions, excellent qualitative agreement is shown between the CFD field plots and the corresponding dye-flow snapshots. Examining the results for the QSTAT-derived motion, it is shown that the wake vorticity for the QSTAT-derived motion is very weak in comparison with the pure-plunge case. The reason for this becomes clear from a study of Eq. (3) for pitch–plunge $C_l$ from QSTAT and the circulatory contributions to the overall $C_l$ from Theodorsen's theory (Eq. (4)). It is shown that when QSTAT is used for pitch–plunge cancellation, the resulting motion, when analyzed using Theodorsen's method, will have zero circulatory $C_l$. The net $C_l(t)$ for this motion from Theodorsen's method will only have two contributions: a constant circulatory contribution from $C_{l_{ss}}$ and a nonconstant $C_l(t/T)$ that is entirely due to the noncirculatory contribution. Because the circulatory contribution is constant, the bound circulation $\Gamma(t)$ for the airfoil is a constant. As a consequence, there is no vorticity shed in the wake, because the wake vorticity depends on $\partial\Gamma/\partial t$. Thus, the QSTAT-derived motion for pitch–plunge cancellation results in a cancellation of the wake vorticity, even though the motion results in a nonconstant $C_l(t/T)$ from the noncirculatory contribution.

Examining the field plots and dye-flow results for the Theodorsen approach-derived motion, it is shown that, unlike with the QSTAT approach, the wake has nonzero vorticity, even though the $C_l(t/T)$ is close to being constant. The nearly constant value of $C_l(t/T)$ results from the variations in circulatory part canceling out the variations in the noncirculatory part. Because the wake vorticity depends only on the circulatory part, the vorticity in the wake is nonzero.

Comparison of the results for the two combined pitch–plunge motions brings out the importance of the noncirculatory contributions to the lift generated by the airfoil motion. With the QSTAT approach, variations in the circulatory portion are canceled out, resulting in near-zero vorticity in the wake. However, the noncirculatory terms still contribute to variations in the $C_l(t)$. With the Theodorsen approach, on the other hand, the variations in the net $C_l(t)$ are brought close to zero, but wake vorticity is present because of variations in the circulatory contribution to lift.

Of particular interest is that the two analytical approaches are shown to be surprisingly accurate in their prediction of flow characteristics for the pitch–plunge motions, in which the moderately large reduced frequencies and nondimensional amplitudes and low Reynolds numbers bring into question the validity of mathematical assumptions in the classical theories. The results of zero wake strength for the QSTAT-derived pitch–plunge combination and zero $C_l(t)$ for the Theodorsen-derived combination support the validity of superposition, even though the flows are intuitively nonlinear.

### B. Case Study 2

In this case study, the same plunge motion from case 1 (labeled 2A for convenience) is considered. Equivalent pitch motions, with the pivot-point location instead at three-quarter-chord, were derived using the two approaches. These were then used to derive two pitch–plunge combination motions for lift cancellation. The pitch motion from QSTAT is shown to result in a large amplitude of 22.5 deg for this pivot-point location.

Figure 10 shows the vorticity-field plots and dye-flow snapshots for the pure-plunge and pure-pitch cases for $t/T$ of 0 and 1/2. The large pitch amplitude in the QSTAT-derived pitch motion with the pivot location at the three-quarter-chord is shown to result in large leading-edge vortex structures. Unlike case 1, the flowfields of the pitch motions have no similarity with either the wake or the surface flowfield of the pure-plunge case. Figure 11 shows the vorticity plots and dye-flow snapshots for the combination motions. The QSTAT-derived combination motion exhibits the large leading-edge vortex structures shown in the corresponding pure-plunge motion. These do not appear to convect to the trailing wake, however, which has weak vortex structures.

Figure 12 presents the $C_l$–time history plots from Theodorsen's theory, CFD, and experiment for the pure plunge and the two pitch–plunge combinations. For the pure-plunge and Theodorsen-derived pitch–plunge motions, theory, CFD, and experiment are shown to be in excellent agreement. The peak-to-peak amplitude $\Delta C_l$ is shown to be small for the Theodorsen-derived pitch–plunge combination, almost one-tenth of that for the pure-plunge motion. This shows that

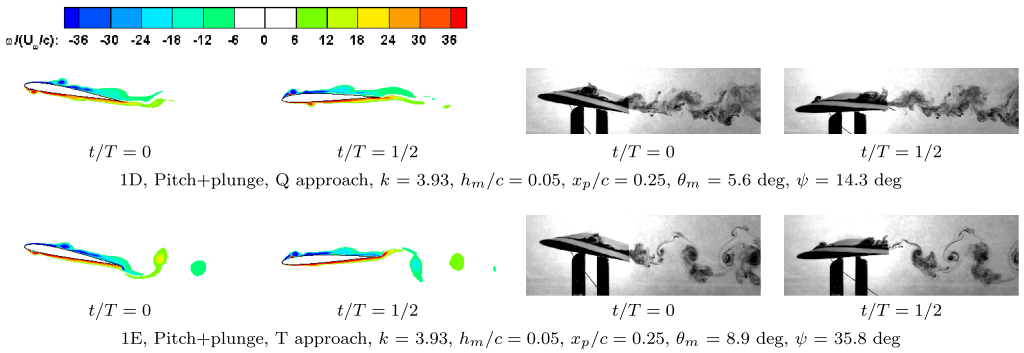


**Fig. 9 Cases 1D, 1E: vorticity-field plots from CFD (left) and dye-flow visualization (right).**

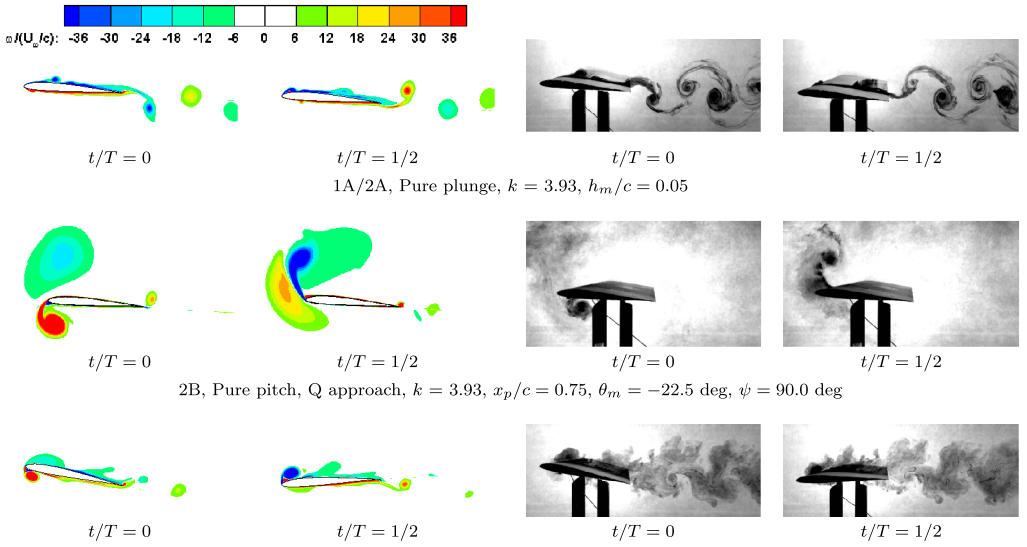


**Fig. 10 Cases 1A/2A, 2B, 2C: vorticity-field plots from CFD (left) and dye-flow visualization (right).**

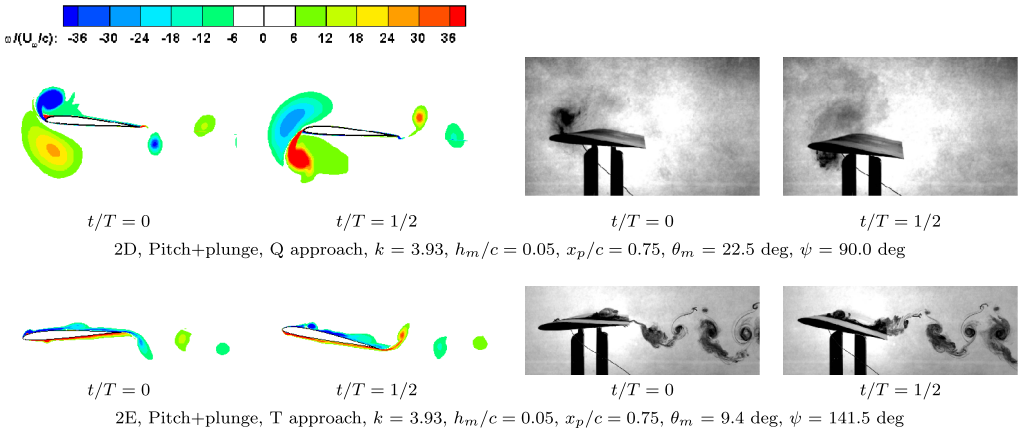


**Fig. 11 Cases 2D, 2E: vorticity-field plots from CFD (left) and dye-flow visualization (right).**

Theodorsen's theory is effective at achieving lift cancellation for this case study.

In contrast, for the QSTAT-derived pitch–plunge motion, the agreement between CFD, experiment, and theory is poor. In particular, predictions from theory deviate significantly from CFD and experiment. In an effort to understand the reason for the poor agreement, we recall that because the circulatory lift is canceled for this motion, the sinusoidal variation of $C_l(t/T)$ from theory is entirely from the noncirculatory contribution, which is added to the small constant offset due to the steady-state $C_l$. As a result of the large pitch amplitude and the large pitch rate about the three-quarter-chord location combined with the plunge, viscous effects are significant. This case clearly has strong flow separation, and it is therefore not surprising that the circulatory portion of Theordorsen's formula, with its attached-flow assumption, fails. To be more precise, the flow separation is not regularized by the presence of tight leading-edge vortices, which, in our conjecture, correlates with the maintenance of a trailing-edge Kutta condition and strong bound vorticity. Instead, the massive flow separation invalidates the bound-vorticity model in the circulatory portion of Theodorsen's formula, and this portion fails outright. However, it is interesting to note that at the times when the noncirculatory contributions to $C_l$ are large, at $t/T = 0.25$ and 0.75 for this case, theory agrees well with CFD and experiment. When the noncirculatory contribution to $C_l$ goes to zero, at $t/T = 0$ and 0.5, the only contribution to $C_l$ is from viscous corrections to what would have been zero circulatory $C_l(t)$ in inviscid flow. It is at these points in the periodic $C_l$ variation that the results from CFD and experiment

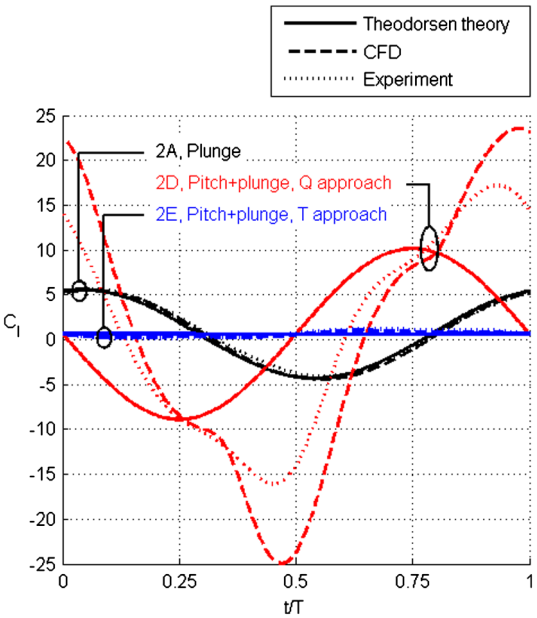


**Fig. 12 $C_l(t)$ distributions from Theodorsen's theory, CFD, and experiment for the baseline pure-plunge motion and the two pitch–plunge combination motions in case 2.**

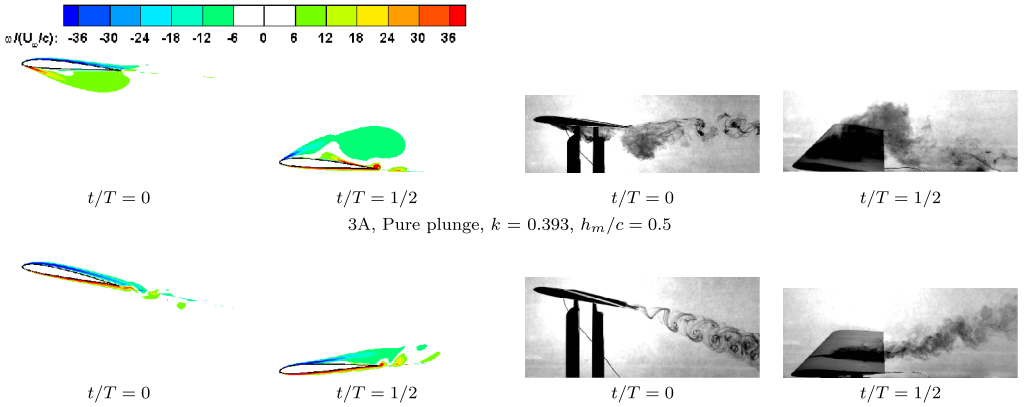


**Fig. 13 Cases 3A, 3E: vorticity-field plots from CFD (left) and dye-flow visualization (right).**

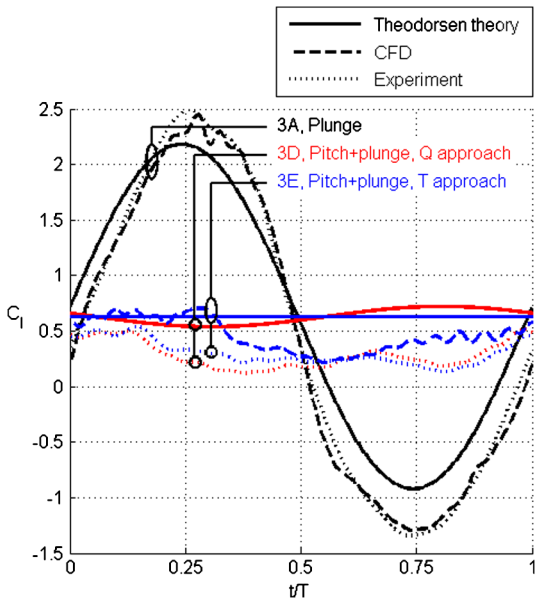


**Fig. 14 $C_l(t)$ distributions from Theodorsen's theory, CFD, and experiment for the baseline pure-plunge motion and the two pitch–plunge combination motions in case 3.**

have maximum deviation from theory. These results bring out the important role played by the noncirculatory contribution to the total lift in determining the effectiveness of linear theory. When the noncirculatory contribution is a large fraction of the total $C_l$ (where total $C_l$ is the sum of the noncirculatory $C_l$, the circulatory $C_l$ in inviscid flow, and the viscous correction to the inviscid circulatory $C_l$), viscous effects do not make a significant contribution and linear theory could work quite well. When the noncirculatory contribution is a small fraction of the total $C_l$, viscous effects could significantly affect the total $C_l$, resulting in inadequate prediction effectiveness of linear theory.

As shown for case 1, lift cancellation is not achieved with the QSTAT-derived combination motion; for case 2, the $C_l$ amplitude for the QSTAT-derived combination motion is nearly four times that of the pure-plunge case. On the other hand, the Theodorsen-derived combination motion is shown to be effective at reducing the $C_l$ amplitude to less than one-tenth of that for the pure-plunge motion. The two matching approaches are also largely successful at achieving the desired objectives for this case study: weak vorticity in the wake despite the presence of strong leading-edge vortex structures for QSTAT and lift cancellation for Theodorsen.

### C. Case Study 3

In this case study, the reduced frequency is decreased to one-tenth of that used in case 1 and the nondimensional amplitude of the plunge motion is increased 10 times. This results in $kh_m/c$ remaining unchanged from that of case 1, which also keeps the Strouhal number based on plunge amplitude unchanged. The pivot-point location is the same as that for case 1, i.e., at $c/4$. For this low value of $k$, the relative contribution of noncirculatory loads is small. As a result, the QSTAT and Theodorsen approaches give nearly the same values for pitch amplitude and phase angle. In other words, matching the circulatory portion of the lift is nearly the same as matching the total lift between plunge and pitch.

Figure 13 shows the vorticity plots and dye-flow snapshots for the pure-plunge motion and the Theodorsen-derived combination motion. The qualitative agreement between CFD and experiment is shown to be good. It is also shown that this plunge motion results in large vortical structures being generated at the leading edge and shed periodically. Figure 14 shows the $C_l$ time histories from theory, CFD, and experiment for the pure plunge and the two pitch–plunge combinations. The lift–time history for the plunge motion is shown to have noticeable deviations from a sinusoidal shape. This is a result of the large vortical structures shown in the flowfield plots. The QSTAT and Theodorsen pitch–plunge combinations have $\Delta C_l$ values that are approximately one-fifth and one-tenth, respectively, of the pure plunge $\Delta C_l$. For this study, the lift cancellation using the Theodorsen approach is not as successful as for the earlier cases, but is still reasonably effective.

### D. Case Study 4

In this case study, the reduced frequency is double that used in case 1 and the amplitude of the plunge motion is half, resulting in $kh_m/c$ (and the Strouhal number based on plunge amplitude) remaining unchanged. The pivot-point location is the same as that for case 1, i.e., at $c/4$.

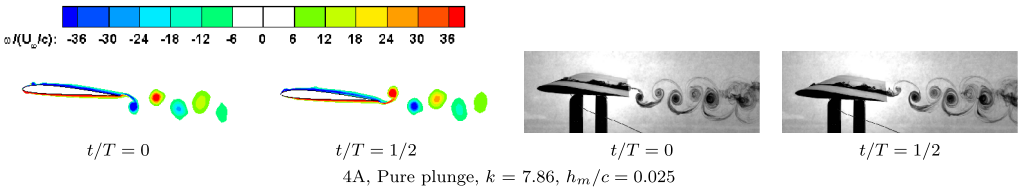


**Fig. 15 Case 4A: vorticity-field plots from CFD (left) and dye-flow visualization (right).**

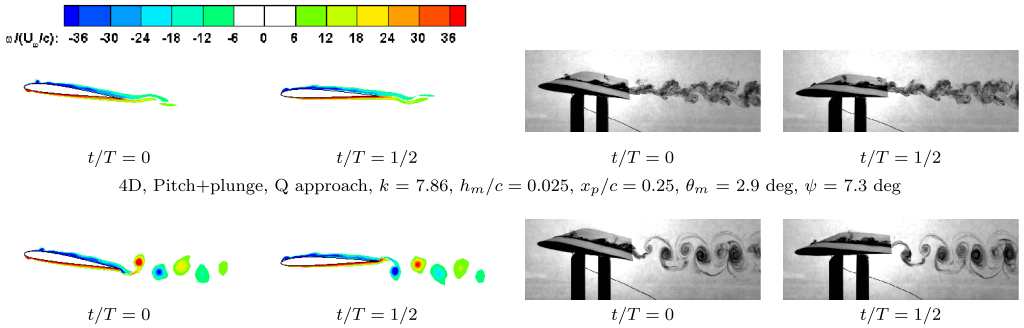


**Fig. 16 Cases 4D, 4E: vorticity-field plots from CFD (left) and dye-flow visualization (right).**

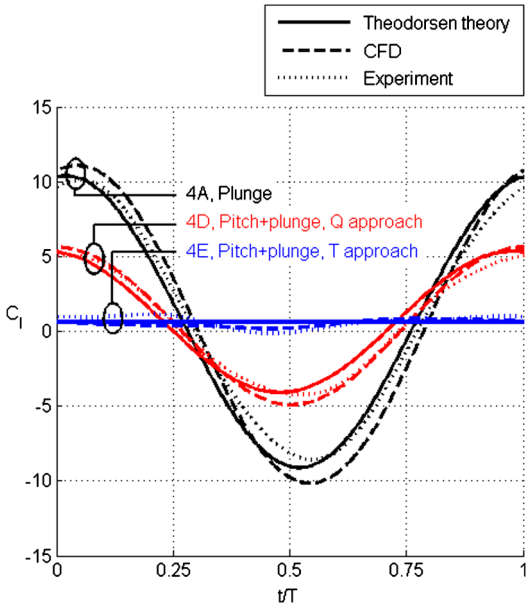


**Fig. 17 $C_l(t)$ distributions from Theodorsen's theory, CFD, and experiment for the baseline pure-plunge motion and the two pitch–plunge combination motions in case 4.**

Figure 15 shows the vorticity plots from CFD and dye-flow snapshots for the pure-plunge motion. The qualitative agreement between CFD and experiment is shown to be excellent. Figure 16 shows the vorticity plots and dye-flow snapshots for the QSTAT- and Theodorsen-derived pitch–plunge combinations. Again qualitative comparison between CFD and experiment is excellent. The QSTAT combination motion is shown to result in weak vorticity in the wake, which is not true for the Theodorsen-derived combination motion. Figure 17 shows the $C_l$ time histories from theory, CFD, and experiment for the pure plunge and the two pitch–plunge combinations. Although the QSTAT-derived combination motion has a $\Delta C_l$ that is about half that of the pure-plunge motion, the Theodorsen-derived combination motion has a $\Delta C_l$ that is just 4% of that shown for the pure-plunge motion.

### E. Case Study 5

This case study is the first of three that comprise the higher-Strouhal-number set. The motion parameters for the pure plunge for this case study were chosen to explore the limits of superposition, while staying within the limits of the pitch–plunge rig of the experimental setup in the water tunnel. As with case 3, the motion parameters for pitch from QSTAT are close to those from Theodorsen. This can be attributed to a smaller value of $k$ compared with case 1. Results are not presented for the QSTAT-derived combination motion for this and the remainder of the cases, as it is clear that the QSTAT approach is not successful at canceling lift.

Figure 18 shows the vorticity plots and dye-flow snapshots for the pure-plunge and Theodorsen-derived combination motions. The large plunge amplitude results in formation of large vortex structures for the pure-plunge case. In the Theodorsen-derived pitch–plunge motion case, the wake appears to have weak vorticity distribution. Figure 19 shows the $C_l$–time history for the pure plunge and the two pitch–plunge combinations. The predictions for the pure-plunge case from CFD and experiment are close to each other, but deviate noticeably from theory. Also shown is that lift cancellation with the Theodorsen combination motion is not as effective as for the earlier case studies; $\Delta C_l$ for this combination motion is approximately 40% of that for the pure-plunge motion. As a consequence of the large amplitude and large Strouhal number, this case study forms a good test of the limits of superposition.

The lack of effectiveness of the Theodorsen approach in canceling lift, in comparison with cases 1–4, motivated cases 6 and 7, in which

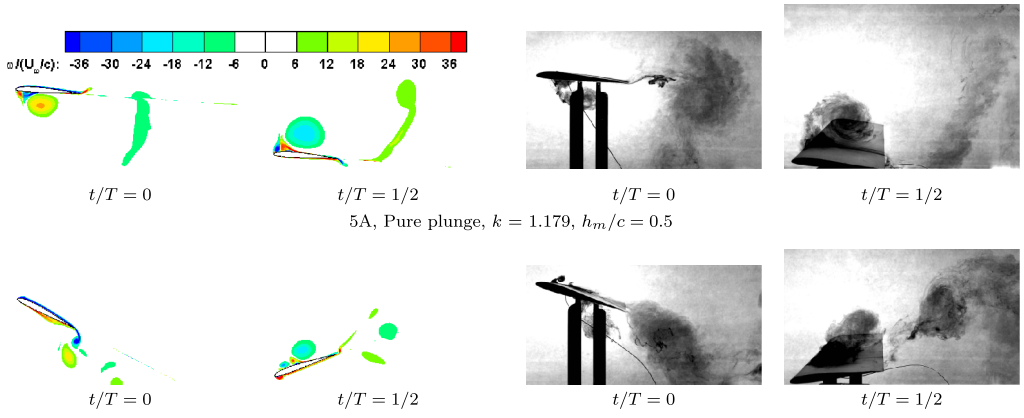


**Fig. 18 Case 5A, 5E: vorticity-field plots from CFD (left) and dye-flow visualization (right).**

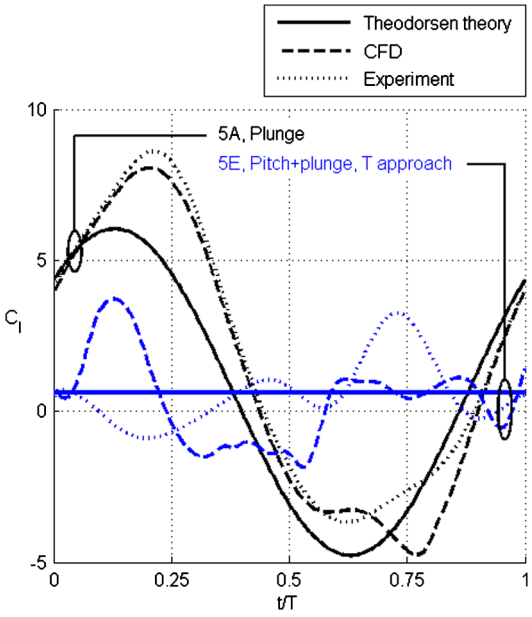


**Fig. 19 $C_l(t)$ distributions from Theodorsen's theory, CFD, and experiment for the baseline pure-plunge motion and the pitch–plunge combination motion in case 5.**

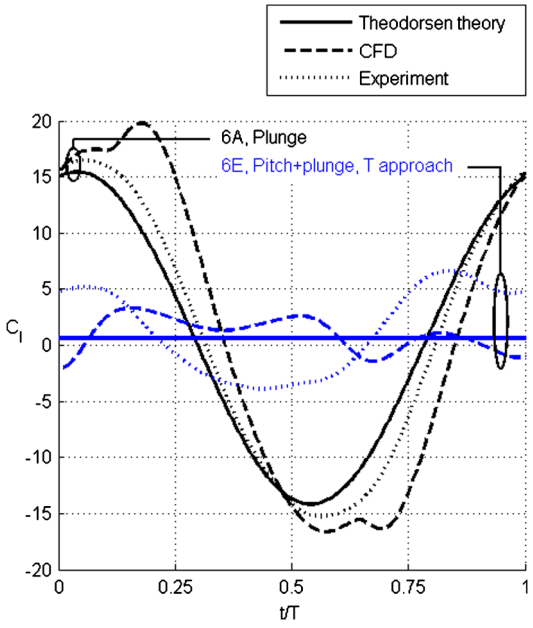


**Fig. 20 $C_l(t)$ distributions from Theodorsen's theory, CFD, and experiment for the baseline pure-plunge motion and the pitch–plunge combination motion in case 6.**

the Strouhal number was maintained at 0.375, but plunge amplitude was varied.

### F. Case Study 6

Having shown the demonstrable breakdown of lift cancellation in the Theodorsen-derived pitch–plunge combined motion of case 5, we now consider whether improvement is possible by taking smaller amplitude (and higher frequency) at the same Strouhal number. In this case study, Strouhal number was maintained from case 5, but plunge amplitude was reduced to 30% of that used in case 5. Figure 20 presents the $C_l$ distributions from theory, CFD, and experiment for the pure-plunge and Theodorsen-derived pitch–plunge combination motions. Experiment and theory for the pure-plunge motion are shown to agree fairly well, with CFD showing some departure from these $C_l$ distributions. The vorticity plots and dye-flow snapshots, shown in Fig. 21 for the pure-plunge and Theodorsen-derived combination motions, continue to show good qualitative agreement between CFD and experiment, with shedding of leading-edge vortex structures shown in both pure-plunge and the combination motions. Deviation in CFD-predicted $C_l(t/T)$ from experiment can be attributed to the failure of 2-D computation to properly capture the 3-D vortex-stretching behavior. Lacking 3-D computations, the current results can neither confirm nor deny this hypothesis. However, for evidence of spurious vortex formation in a 2-D vs a 3-D computation, one may refer, for example, to Granlund et al. [21].

The question remains as to why there is disagreement between 2-D CFD and Theodorsen's theory. We suggest an explanation by recalling that Theodorsen's formula makes no attempt at resolving the flowfield in general or vortex production/growth/shedding in particular. The fact that it is oblivious to the suction contribution of leading-edge vortices to the lift history suggests that this contribution is small if and when Theodorsen's formula has good agreement with experiment. The CFD, on the other hand, does attempt to resolve vortex formation, growth, and shedding, but perhaps does so incorrectly, in part because of its limitation to 2-D and failure to include effects of vortex-stretching. The issue, we suggest, is that an erroneous resolution of vortices is sometimes inferior to ignoring such vortices completely, in regard to prediction of lift-coefficient history. The presence of the leading-edge vortices in the actual flow may be more important for maintenance of a trailing-edge Kutta condition than vortex-induced lift per se. This is our supposition for what happens in those cases in which Theodorsen's formula and experiment track each other closely, and the CFD result is the outlier.

### G. Case Study 7

In this final case study, Strouhal number was again maintained from case 5, but plunge amplitude was further reduced to 15% of that

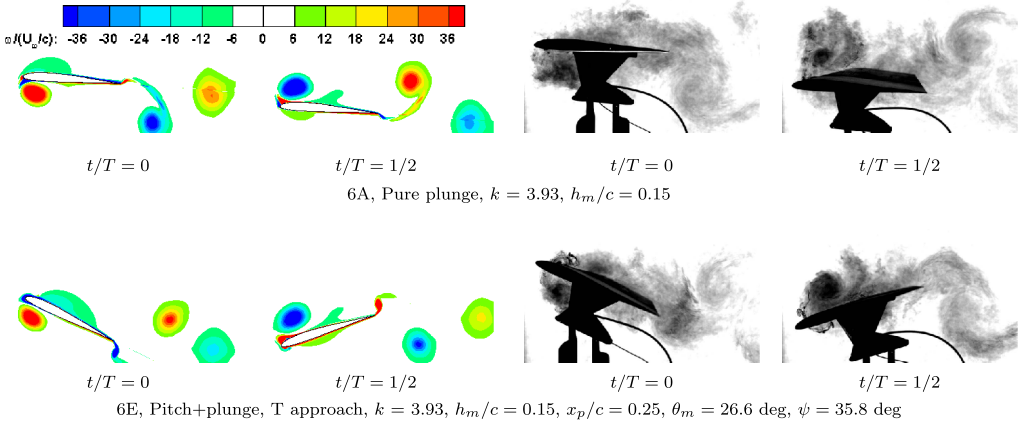


**Fig. 21 Cases 6A, 6E: vorticity-field plots from CFD (left) and dye-flow visualization (right).**

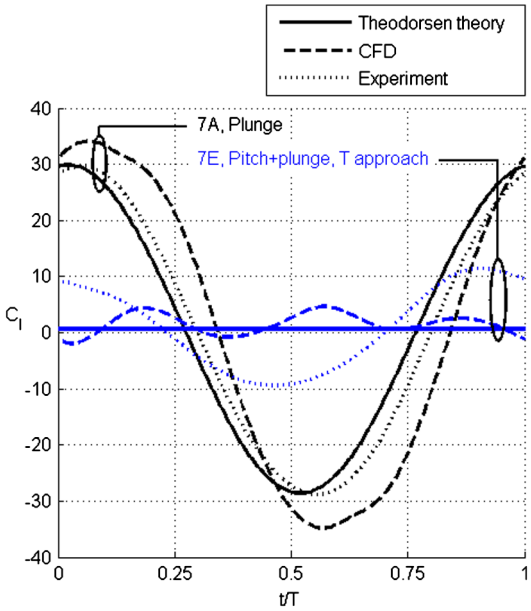


**Fig. 22 $C_l(t)$ distributions from Theodorsen's theory, CFD, and experiment for the baseline pure-plunge motion and the pitch–plunge combination motion in case 7.**

used in case 5. Figure 22 presents the $C_l$ distributions from theory, CFD, and experiment for the pure-plunge and Theodorsen-derived pitch–plunge combination motions, and Fig. 23 presents the vorticity plots and dye-flow snapshots. The trends are quite similar to case 6, with a little better effectiveness of the Theodorsen approach in canceling lift.

### H. Summary

A shorthand for the effectiveness of Theodorsen's method to generate a sinusoidal pitch that cancels lift history of a prescribed sinusoidal plunge is to consider the peak-to-peak lift amplitudes of the original plunging motion vs those of the derived pitch–plunge combination. The ratio of the latter to the former is given in Table 2. Such a comparison disregards whether the lift history of the pitch–plunge combination is itself sinusoidal, or whether it contains higher harmonics; but it does show that case 5 (high Strouhal number and maximal amplitude) is a clear outlier in its large ratio of peak-to-peak residual lift to the respective pure-plunge case's peak-to-peak lift. There is also a general trend that for a given Strouhal number, the smaller the prescribed plunge amplitude, the better the pitch–plunge lift cancellation. This is a direct consequence of the relative balance of circulatory and noncirculatory lift contributions; for constant Strouhal number as $k$ increases and $h$ decreases, the noncirculatory lift contribution becomes relatively larger. This is evidently correctly

**Table 2 Effectiveness of the Theodorsen approach when canceling $C_l(t/T)$[a]**

| Case | $k$ | $h_m/c$ | $St$ | $x_p/c$ | $\Delta C_{lE}$[b] | $\Delta C_{lE}/\Delta C_{lA}$[b] |
|---|---|---|---|---|---|---|
| 1 | 3.930 | 0.050 | 0.125 | 0.25 | 0.59 (1.08) | 0.06 (0.11) |
| 2 | 3.930 | 0.050 | 0.125 | 0.75 | 0.81 (1.07) | 0.08 (0.11) |
| 3 | 0.393 | 0.500 | 0.125 | 0.25 | 0.49 (0.41) | 0.13 (0.11) |
| 4 | 7.860 | 0.025 | 0.125 | 0.25 | 0.66 (1.28) | 0.03 (0.07) |
| 5 | 1.179 | 0.500 | 0.375 | 0.25 | 5.58 (4.15) | 0.44 (0.34) |
| 6 | 3.930 | 0.150 | 0.375 | 0.25 | 5.35 (10.51) | 0.15 (0.33) |
| 7 | 7.860 | 0.075 | 0.375 | 0.25 | 6.62 (20.87) | 0.10 (0.36) |

[a]Measured by the peak-to-peak $C_l$ amplitude for the Theodorsen pitch–plunge motion $\Delta C_{lE}$ as a ratio of the peak-to-peak $C_l$ amplitude for the corresponding pure-plunge motion $\Delta C_{lA}$.
[b]From CFD (experiment).

captured by Theodorsen's formula, even for flows with large separation, strongly nonplanar wakes, and leading-edge vortices. Thus, the higher the relative noncirculatory lift contribution, the lower the residual peak-to-peak lift in the Theodorsen-derived pitch–plunge combined motion.

One may wonder whether the choice of pitch amplitude and phase angle from Theodorsen's formula is the optimal scheme for matching lift history to that of the prescribed plunge. That is, might there be a scenario in which Theodorsen's method yields poor lift cancellation in combined pitch–plunge, but some other scheme succeeds? If the answer is in the affirmative, then this would mean that linear superposition remains essentially valid even if a planar-wake attached-flow theory (Theodorsen's) fails. Granlund et al. [3] investigated this by trial-and-error choices of pitch amplitude and phase with the prescriptions from Theodorsen's formula as a departure point. In summary, wherever Theodorsen's method already worked reasonably well, such as our cases 1–4 above, minor further improvements in lift-history cancellation were possible. And where Theodorsen's method failed, such as our case 5 above, other choices of amplitude/phase differences were not significantly better. We therefore conclude that the success or failure of Theodorsen's method is a useful proxy for the broader question of when linear superposition itself holds or fails.

## VII. Conclusions

Linear predictive methods in two-dimensional aerodynamics (which assume planar wakes, fully attached flow, a trailing-edge Kutta condition, and enforcement of boundary conditions on the airfoil chord line) are conceptually attractive for their simplicity. Here, two linear approaches are examined: the quasi-steady theory (which includes plunge-induced angle of attack, geometric pitch angle, and pitch-rate effects) and Theodorsen's formula (which includes the contribution of a planar-wake/vortex sheet and noncirculatory lift, or apparent mass). The proxy for validity of linear theories is the assessment of how, given a prescribed harmonic pure-plunge motion, one can find a pure-pitch motion that yields identical

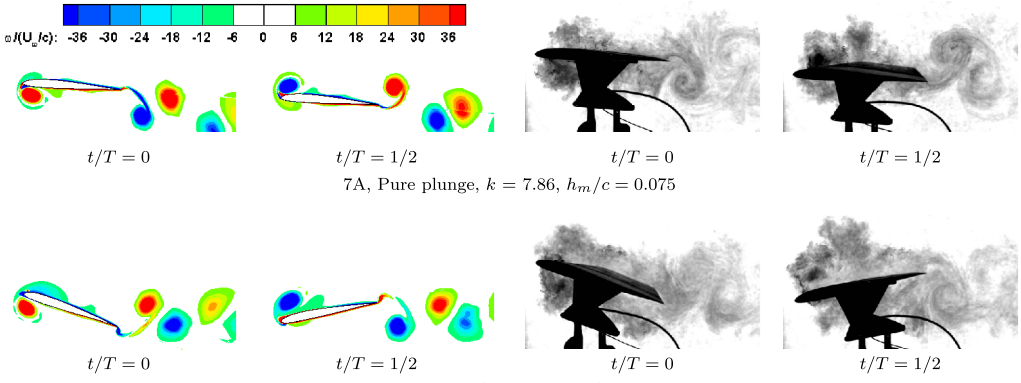


**Fig. 23 Cases 7A, 7E: vorticity-field plots from CFD (left) and dye-flow visualization (right).**

lift-coefficient history or, alternatively, whether one can find pitch conditions such that the combined pitch–plunge motion will identically cancel lift history.

Lift-coefficient computations with a 2-D RANS approach were found to agree reasonably well with direct measurement of lift history using a force balance in a water tunnel, with areas of disagreement primarily where there are large leading-edge vortices and the 2-D computation fails to properly capture the vortex-stretching term. The experimental–computational lift comparison was complemented by dye injection in the water tunnel, as a qualitative surrogate for vorticity measurement, and out-of-plane vorticity contours from the computation, which, as with the lift history, showed good agreement. One can therefore surmise that the experiment and computation are jointly a schema for assessing the lift predictions of the linear theories.

Two Strouhal numbers were considered: 0.125 and 0.375. In each, several cases were considered in which reduced frequency was raised, whereas the reduced amplitude was lowered, and vice versa, such that their product was constant. Also considered were pitch-rate effects, in that the choice of pitch pivot point will affect the pitch-rate contribution to lift. Quasi-steady airfoil theory generally fails to give good lift prediction for the cases examined here, which is only to be expected, as this theory does not capture the noncirculatory contributions. But Theodorsen's method was observed to have considerable, and perhaps surprising, resilience in finding pitch–plunge lift cancellation, despite application to cases in which its mathematical assumptions are clearly violated, in the sense of a nonplanar wake and large leading-edge flow separation. This is for two reasons: first, even in cases of substantial leading-edge vortex formation, a trailing-edge Kutta condition can still remain valid, whence the bound-vorticity prediction is approximately true; second, and more important, is the role of noncirculatory force. When noncirculatory lift contributions dominate the circulatory contributions (both bound vorticity and shed vorticity), Theodorsen's method is successful. It fails demonstrably at high Strouhal number if the reduced amplitude is also large, because the noncirculatory contribution does not dominate there, and the trailing-edge Kutta condition is violated. It also fails for cases in which the leading-edge displacement is large, again because of strong leading-edge vortices. This is the scenario in which the pitch pivot point is taken far aft on the chord, even if the baseline plunge case is of moderate amplitude. If one considers amplitude to refer to either pitch or plunge displacement, then the product of Strouhal number and reduced amplitude defines the bound of validity of linear methods in unsteady 2-D aerodynamics and of linear superposition in particular.

## Acknowledgments

The authors wish to gratefully acknowledge the support of the U.S. Air Force Office of Scientific Research through grant FA 9550-10-1-0120 with Program Manager Douglas Smith.

## References

[1] McGowan, G. Z., Gopalarathnam, A., Ol, M. V., Edwards, J. R., and Fredberg, D., "Computation vs. Experiment for High-Frequency Low-Reynolds Number Airfoil Pitch and Plunge," AIAA Paper 2008-0653, Jan. 2008.

[2] McGowan, G. Z., Gopalarathnam, A., Ol, M. V., and Edwards, J. R., "Analytical, Computational, and Experimental Investigations of Equivalence Between Pitch and Plunge Motions for Airfoils at Low Reynolds Numbers," AIAA Paper 2009-0535, Jan. 2009.

[3] Granlund, K., McGowan, G. Z., Ol, M. V., Gopalarathnam, A., and Edwards, J. R., "The Validity Bounds of Analytical Force and Moment Predictions for Pitch and Plunge Oscillating Low Reynolds Number Airfoil," AIAA Paper 2010-8126, Aug. 2010.

[4] Selig, M. S., Donovan, J. F., and Fraser, D. B., *Airfoils at Low Speeds*, Soartech 8, SoarTech, Virginia Beach, VA, 1989.

[5] Ol, M., McAuliffe, B. R., Hanff, E., Scholz, U., and Kähler, C., "Comparison of Laminar Separation Bubble Measurements on a Low Reynolds Number Airfoil in Three Facilities," AIAA Paper 2005-5149, June 2005.

[6] Lian, Y., Ol, M., and Shyy, W., "Comparative Study of Pitch–Plunge Airfoil Aerodynamics at Transitional Reynolds Number," AIAA Paper 2008-0652, Jan. 2008.

[7] Theodorsen, T., "General Theory of Aerodynamic Instability and the Mechanism of Flutter," NACA Rept. 496, 1935.

[8] Krist, S. L., Biedron, R. T., and Rumsey, C. L., "CFL3D User's Manual," NASA TM 208444, 1998.

[9] Ol, M. V., "Vortical Structures in High Frequency Pitch and Plunge at Low Reynolds Number," AIAA Paper 2007-4233, June 2007.

[10] Leishman, J. G., *Principles of Helicopter Aerodynamics*, Cambridge Aerospace Series, Cambridge Univ. Press, New York, 2002.

[11] Spalart, P. R., and Allmaras, S. R., "A One-Equation Turbulence Model for Aerodynamic Flows," AIAA Paper 92-0439, 1992.

[12] Ol, M., Bernal, L., Kang, C.-K., and Shyy, W., "Shallow and Deep Dynamic Stall for Flapping Low Reynolds Number Airfoils," *Experiments in Fluids*, Vol. 46, No. 5, May 2009, pp. 883–901. doi:10.1007/s00348-009-0660-3

[13] Visbal, M., "High-Fidelity Simulation of Transitional Flows past a Plunging Airfoil," *AIAA Journal*, Vol. 47, No. 11, Nov. 2009, pp. 2685–2697. doi:10.2514/1.43038

[14] Bartels, R. E., "Finite Macro-Element Mesh Deformation in a Structured Multi-Block Navier–Stokes Code," NASA TM 2005, 2005.

[15] McGowan, G. Z., "Analytical and Computational Investigations of Airfoils Undergoing High-Frequency Sinusoidal Pitch and Plunge Motions at Low Reynolds Numbers," Ph.D. Thesis, North Carolina State Univ., Raleigh, NC, Aug. 2008.

[16] Lomax, B., "Indicial Aerodynamics," *Manual on Aeroelasticity*, AGARD Rept. 578, Neuilly-sur-Seine, France, 1968, Chap. 6.

[17] Edwards, J. R., and Thomas, J. L., "Development and Investigation of $\mathcal{O}(\mathrm{N\,m^2})$ Preconditioned Multigrid Solvers for the Euler and Navier–Stokes Equations," AIAA Paper 99-3263, 1999.

[18] Smits, A. J., and Lim, T. T. (ed.), *Flow Visualization: Techniques and Examples*, Imperial College Press, London, 2000, Chap. 3.

[19] Taylor, G. K., Nudds, R. L., and Thomas, A. L. R., "Flying and Swimming Animals Cruise at a Strouhal Number Tuned for High Power Efficiency," *Nature*, Vol. 425, No. 6959, 2003, pp. 645–747. doi:10.1038/425645a

[20] Platzer, M., Jones, K., Young, J., and Lai, J., "Flapping Wing Aerodynamics: Progress and Challenges," *AIAA Journal*, Vol. 46, No. 9, 2008, pp. 2136–2149. doi:10.2514/1.29263

[21] Granlund, K., Ol, M. V., Garmann, D., Visbal, M., and Bernal, L., "Experiments and Computations on Abstractions of Perching," AIAA Paper 2010-4943, Aug. 2010.

F. Coton
*Associate Editor*